Supplemental Material for "Thermal Critical Points and Quantum Critical End Point in the Frustrated Bilayer Heisenberg Antiferromagnet"

J. Stapmanns, P. Corboz, F. Mila, A. Honecker, B. Normand, and S. Wessel

S1. QMC sign problem

The accuracy of our thermodynamic calculations (Figs. 2 and 3 of the main text) is attainable because the FFB is amenable to sign-problem-free QMC simulations. These are based upon the very simple form of the Hamiltonian at $J_\times = J_\parallel$ [Eq. (2) of the main text] when expressed in the dimer spin basis,

$$\vec{T}_i = \vec{S}_{i,1} + \vec{S}_{i,2}, \tag{S1}$$

of the $J_\perp$ bonds. On moving away from this fully frustrated limit, the Hamiltonian takes the form [S1, S2]

$$H = \tfrac{1}{2}(J_\parallel + J_\times)\sum_{i,j}\vec{T}_i\cdot\vec{T}_j + \tfrac{1}{2}(J_\parallel - J_\times)\sum_{i,j}\vec{D}_i\cdot\vec{D}_j + J_\perp\sum_i[\tfrac{1}{2}\vec{T}_i^2 - S(S+1)], \tag{S2}$$

which for $J_\times \neq J_\parallel$ contains the spin-difference operators

$$\vec{D}_i = \vec{S}_{i,1} - \vec{S}_{i,2}. \tag{S3}$$

The DD terms cause the sign problem to reappear.

As discussed for the frustrated ladder in Ref. [S1], a 1D system with only DD (and no DT) terms has only a mild sign problem over much of the $J_\times \neq J_\parallel$ phase diagram. This can be traced to the fact that QMC configurations with a negative sign are rare with respect to the full configuration space and are completely absent for a ladder with open boundary conditions [S2]. For a finite ladder with periodic boundary conditions, negative-weight configurations contain a string of bond operators, when formulated within the stochastic series expansion, that spans the full spatial extent of the system, and the probability for such configurations is suppressed strongly by increasing the system size at low temperatures.

By contrast, negative-weight QMC configurations occurring in the frustrated bilayer may contain bond operators from only a small part of the lattice, i.e., in 2D these configurations need not span the system and do appear with open boundary conditions. Hence we do suffer from strong sign problems in our QMC simulations sufficiently far from the fully frustrated limit. To examine the onset of the sign problem in more detail, we have performed a scan, over the full parameter space of the Hamiltonian in Eq. (S2), to measure the average sign, $\langle\text{sign}\rangle$, of the QMC configurations sampled. The results obtained for a moderate system size, $L = 10$, and at a temperature of $T = 0.05J_\parallel$, are represented by the color scale in Fig. S1. The behavior of $\langle\text{sign}\rangle$ is correlated with the location of the phase boundaries in the ground state (reproduced from Fig. 1 of the main text). Although neither the BAF phase nor the transitions into it are accessible in the dimer basis, the sign problem does remain moderate in large parts of the other two phases.

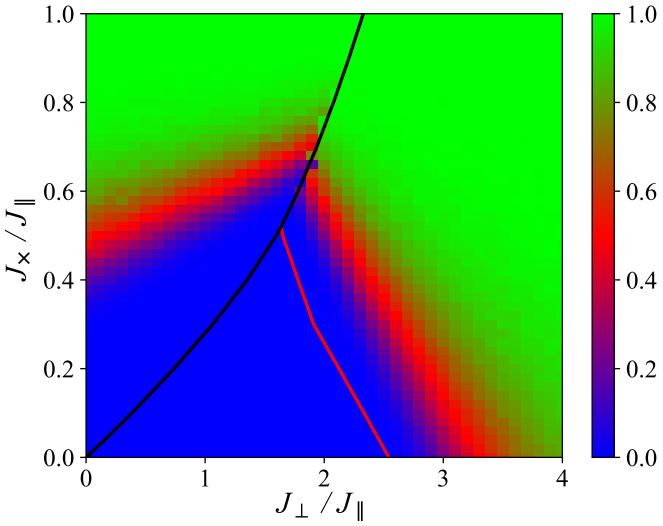

FIG. S1. Calculation of $\langle\text{sign}\rangle$, with $L = 10$ and $T = 0.05J_\parallel$, within a dimer-basis formulation of the QMC algorithm. Solid lines reproduce the phase boundaries shown in Fig. 1 of the main text.

For practical purposes, a value $\langle\text{sign}\rangle \gtrsim 0.1$ can still be tolerated in our QMC simulations, i.e., compensated by increasing the QMC sampling (the CPU time) by a factor of 100. As an example of working at partial frustration, we illustrate our estimation of the critical temperature at frustration ratio $J_\times = 0.7J_\parallel$ (reported in the main text). As in Fig. 2(d) of the main text, we computed the singlet density, ρ_s, at different temperatures as a function of the coupling ratio $J_\perp/J_\parallel$, achieving a maximum system size of $L = 24$. As Fig. S2 makes clear, we observe a clear jump in ρ_s near $J_\perp/J_\parallel = 1.93$ for temperatures $T \leq 0.44J_\parallel$, whereas this quantity exhibits a continuous growth for $T \geq 0.46J_\parallel$. Thus we estimate the location of the critical point at $J_\times = 0.7J_\parallel$ to be $(J_{\perp,I}, T_I) = (1.93(1)J_\parallel, 0.45(1)J_\parallel)$. We comment that the corresponding first-order transition point in the ground state, which we located by our iPEPS calculations, is $J_{\perp,c} = 1.9375(8)J_\parallel$, and hence the finite-$T$ first-order line at $J_\times = 0.7J_\parallel$ shows the same weak T-dependence as at full frustration.

With current computer power it becomes practically impossible to perform reliable QMC simulations beyond

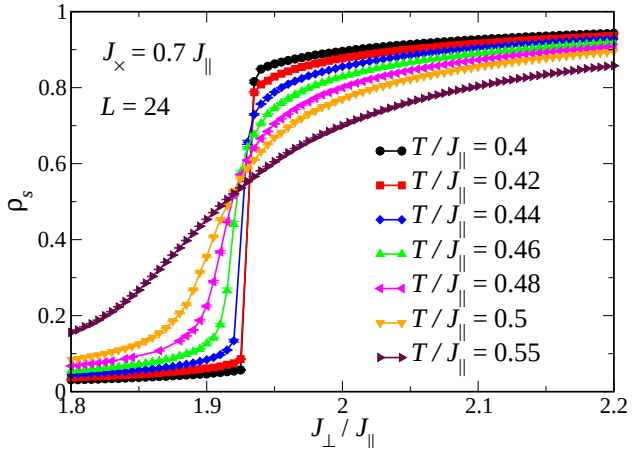

FIG. S2. Singlet density, ρ_s, calculated on a system of size $L = 24$ with frustration ratio $J_\times = 0.7J_\parallel$, shown for different temperatures as a function of coupling ratio $J_\perp/J_\parallel$.

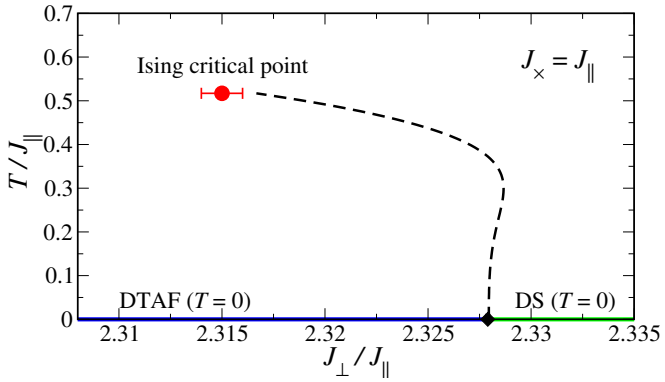

FIG. S3. Phase diagram of the FFB showing in detail the region of the finite-T first-order transition line (dashed). As in Fig. 3(b) of the main text, the red dot marks the Ising critical point, $(J_{\perp,I}, T_I) = (2.315(1)J_\parallel, 0.517(3)J_\parallel)$, computed by QMC and the black dot the QPT at $(J_{\perp,c}, T) = (2.3279(1)J_\parallel, 0)$, taken from Ref. [S5].

the regime represented in red in Fig. S1. In the present case, the sign problem prevents us from studying the region of the QCEP by QMC, and also from following the line of finite-temperature Ising critical points below frustration values $J_\times/J_\parallel \approx 0.7$. For either purpose, accurate thermodynamic studies would require system sizes considerably larger than that used in Fig. S1. For future analysis it may be necessary to investigate whether the sign problem can be alleviated in the vicinity of the QCEP by further optimizing the local computational basis using a more general unitary transformation. We comment in closing that the UFB at $J_\times = 0$ is a bipartite system, which can be studied in detail by QMC simulations in the conventional site basis without encountering a sign problem, and indeed many previous studies of the UFB have been performed in this way, including in Refs. [S3, S4].

S2. Finite-temperature transition line

Here we discuss in detail the form, in the space of coupling ratio and temperature, of the finite-T first-order line in the FFB. As noted in the main text, in general one expects the level crossing between the DT- and DS-dominated phases to move to a different coupling ratio as a function of temperature, which influences the two phases quite differently. However, it is clear in Fig. 3(b) of the main text that the effects of thermal fluctuations are not very strong on the scale of the entire parameter space.

For a full analysis of the problem, we consider the free energies on the two sides of the transition line, $F_1(x,T)$ and $F_2(x,T)$, where $x = J_\perp/J_\parallel$ denotes the coupling ratio in the FFB. Let 1 denote the DTAF phase, which is gapless, and 2 the DS phase, which is gapped. At finite temperature, $F_i(x,T) = E_i(x,T) - TS_i(T)$ $(i = 1, 2)$, where $E_1(x,0)$ and $E_2(x,0)$ are the ground-state energies and we take $S_i(T)$ to be x-independent in the vicinity of the QPT. Because the model is in two spatial dimensions, the specific heat of the DTAF should obey $C_v(T) = aT^2$, whence by integration

$$E_1(x,T) - E_1(x,0) = \tfrac{1}{3}aT^3 \quad \text{and} \quad S_1(T) = \tfrac{1}{2}aT^2,$$

giving to a good approximation

$$F_1(x,T) = E_1(x,0) - \tfrac{1}{6}aT^3.$$

In contrast to these power-law expressions, in the gapped DS phase one expects only exponentially weak changes in $E_2(x,T)$ and $S_2(T)$. By approximating the well-gapped DS state using the response of a single dimer with the same spin gap, Δ, we obtain

$$F_2(x,T) = -T \ln Z_2(x,T)$$

with

$$Z_2(x,T) = \exp[-E_2(x,0)/T] + 3\exp[-(E_2(x,0)+\Delta)/T],$$

leading to

$$F_2(x,T) = E_2(x,0) - T\ln[1 + 3\exp(-\Delta/T)].$$

By equating the two approximate free energies we obtain the location of the first-order transition line from the equation

$$\tfrac{1}{6}aT^3 - T\ln[1 + 3\exp(-\Delta/T)] = E_1(x,0) - E_2(x,0),$$

where a is the coefficient of the specific heat per spin-1 entity in the DTAF, $\Delta = J_\perp$ is the gap in the DS phase, and $E_1(x,0)$ and $E_2(x,0)$ are respectively the zero-temperature energies per dimer of the ordered and gapped phases.

We use the fact that $E_1(x,0)-E_2(x,0)$ is precisely the ground-state energy of the $S=1$ square-lattice antiferromagnet (see Eq. (2) of the main text), and take both this value and the coefficient $a=0.2441$ from the QMC simulations of Ref. [S6]. As Fig. S3 makes clear, these considerations give an excellent account of the position of the finite-T first-order line in the coupling-temperature phase diagram of the FFB. The fundamental features of the line are its vertical approach to $J_{\perp,c}$ as $T\to 0$ and the location of the critical point to the left of the zero-temperature QPT. However, the latter is actually the result of a competition between the power-law terms in $F_1(x,T)$ and the exponential behavior in $F_2(x,T)$, which causes the transition line to rise first to the right (thermal fluctuations favor DTs) before bending back to the left (temperatures higher than $T/J_\parallel\approx 0.3$ favor the DS phase). The crossover temperature appears to depend smoothly on a but to vary linearly with Δ, with a coefficient of approximately 0.15.

We stress once again the very narrow regime of coupling ratios over which these effects take place in the FFB. Nevertheless, the model provides an excellent example of a system in which the interplay of quantum and thermal fluctuations can be studied in the context of a key physical consequence, namely the location of the line of finite-T transitions.

S3. iPEPS

Infinite projected entangled pair states (iPEPS) are a variational tensor-network ansatz which provides an efficient representation of the ground states of 2D systems in the thermodynamic limit [S7–S9]. iPEPS may be considered as a generalization of (infinite) matrix-product states to two dimensions. The ansatz consists of a unit cell of tensors repeated periodically on the lattice. Here we use one tensor per dimer in the bilayer model. Each tensor has one physical index representing the local Hilbert space of the dimer and four auxiliary indices with bond dimension D, which connect to the four nearest-neighbor tensors. By using different unit-cell sizes, iPEPS can represent states of differing broken translational symmetry. We find that a unit cell with 2 tensors arranged in a checkerboard pattern is sufficient to capture all the phases of the frustrated bilayer model.

For the optimization of the iPEPS wave function (i.e., finding the optimal variational parameters) we use both the simple-update approach [S10], in which the truncation of a bond index is based on a local approximation of the state, and by the more accurate, but computationally more expensive, full-update method [S8, S11], where the entire state is taken into account for the truncation. Contraction of the tensor network, required in the full-update method and to compute expectation values, was performed by a variant [S12] of the corner-transfer-matrix renormalization-group method [S13, S14], in which we exploit the U(1) symmetry of the model [S15, S16]. Further details of iPEPS methods may be found in Refs. [S11, S17].

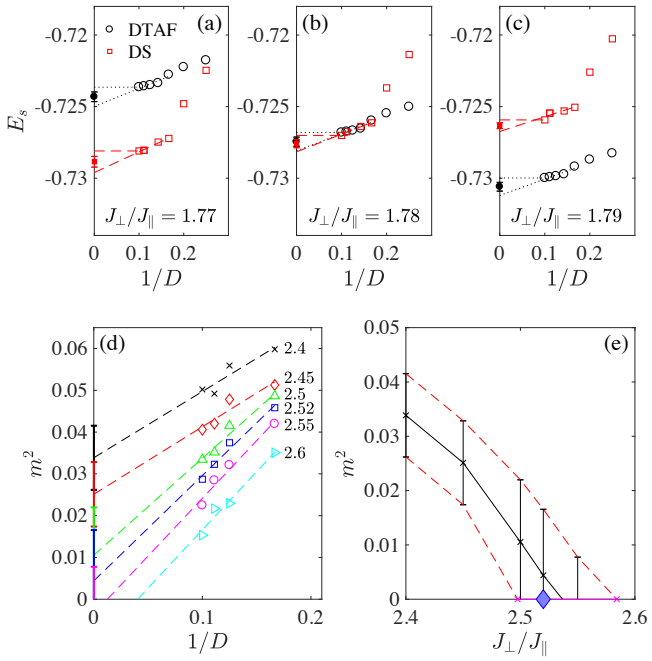

FIG. S4. (a)-(c) Energies of the DTAF and DS states calculated by the simple-update method with $J_\times/J_\parallel=0.6$ for three different values of $J_\perp/J_\parallel$ and shown as functions of the inverse bond dimension. Solid symbols denote the extrapolated estimate in the infinite-D limit. (d) Squared local magnetic moment calculated by the full-update method with $J_\times=0$ for the indicated values of $J_\perp/J_\parallel$ and shown as a function of $1/D$. (e) Extrapolated value of m^2 obtained from panel (d). The blue diamond shows the critical coupling obtained by QMC.

To illustrate the procedure by which we obtain estimates of physical expectation values from calculations with finite bond dimension, Figs. S4(a)-S4(c) show example data for the energies of the competing DTAF and DS states close to first-order QPT for $J_\times/J_\parallel=0.6$ [cf. Fig. 4(a) of the main text]. To estimate the energy in the limit of infinite D, we take the average between the value obtained by linear extrapolation in $1/D$ and the value obtained from our largest D ($=10$). The former typically provides a lower bound, because the energy converges faster than linearly in $1/D$, while the latter is an upper bound. As the error bar we take half the difference between the extrapolation and the upper bound (an approach similar to Ref. [S17]). From the intersection of the energy estimates for the two states, taking the error bars into account, we deduce a critical value $J_\perp/J_\parallel=1.7803\pm 0.0014$. For comparison, the value obtained purely from our $D=10$ data is $J_\perp/J_\parallel=1.7805$, and thus the finite-$D$ error is very small here.

In Fig. S4(d) we show full-update data for the square of the magnetic order parameter in the UFB ($J_\times=0$).

To obtain an estimate in the infinite-D limit, here we use a linear extrapolation in $1/D$ and an error bar given by half the difference between the extrapolated and largest-D values. Although this procedure provides only a rather crude estimate of the order parameter, we stress that it does allow us to determine the location of the continuous BAF-DS phase transition with reasonable accuracy, as shown in Fig. S4(e). In this example we find that the order parameter vanishes at a critical value $J_\perp/J_\parallel = 2.54(4)$, which is fully compatible with the QMC result, $J_\perp/J_\parallel = 2.5220(2)$ [S4].

[S1] S. Wessel, B. Normand, F. Mila, and A. Honecker, SciPost Phys. **3**, 005 (2017).

[S2] F. Alet, K. Damle, and S. Pujari, Phys. Rev. Lett. **117**, 197203 (2016).

[S3] A. W. Sandvik and D. J. Scalapino, Phys. Rev. Lett. **72**, 2777 (1994).

[S4] L. Wang, K. S. D. Beach, and A. W. Sandvik, Phys. Rev. B **73**, 014431 (2006).

[S5] E. Müller-Hartmann, R. R. P. Singh, C. Knetter, and G. S. Uhrig, Phys. Rev. Lett. **84**, 1808 (2000).

[S6] D. C. Johnston, R. J. McQueeney, B. Lake, A. Honecker, M. E. Zhitomirsky, R. Nath, Y. Furukawa, V. P. Antropov, and Y. Singh, Phys. Rev. B **84**, 094445 (2011).

[S7] F. Verstraete and J. I. Cirac, arXiv:cond-mat/0407066.

[S8] J. Jordan, R. Orús, G. Vidal, F. Verstraete, and J. I. Cirac, Phys. Rev. Lett. **101**, 250602 (2008).

[S9] Y. Nishio, N. Maeshima, A. Gendiar, and T. Nishino, arXiv:cond-mat/0401115.

[S10] H. C. Jiang, Z. Y. Weng, and T. Xiang, Phys. Rev. Lett. **101**, 090603 (2008).

[S11] H. N. Phien, J. A. Bengua, H. D. Tuan, P. Corboz, and R. Orús, Phys. Rev. B **92**, 035142 (2015).

[S12] P. Corboz, T. M. Rice, and M. Troyer, Phys. Rev. Lett. **113**, 046402 (2014).

[S13] T. Nishino and K. Okunishi, J. Phys. Soc. Jpn. **65**, 891 (1996).

[S14] R. Orús and G. Vidal, Phys. Rev. B **80**, 094403 (2009).

[S15] S. Singh, R. N. C. Pfeifer, and G. Vidal, Phys. Rev. B **83**, 115125 (2011).

[S16] B. Bauer, P. Corboz, R. Orús, and M. Troyer, Phys. Rev. B **83**, 125106 (2011).

[S17] P. Corboz and F. Mila, Phys. Rev. B **87**, 115144 (2013).